JOURNAL OF GEOPHYSICAL RESEARCH, VOL. 98, NO. B3, PAGES 4423–4435, MARCH 10, 1993

Shear Wave Properties and Seismic Imaging of Mylonite Zones

CAREY L. MCCAFFREE AND NIKOLAS I. CHRISTENSEN

Department of Earth and Atmospheric Sciences, Purdue Rock Physics Laboratory
Purdue University, West Lafayette, Indiana

Major crustal fault zones have displayed high reflectivity on observed compressional reflection profiles and synthetic models of laboratory measurements. This high compressional wave reflectivity suggests that shear waves may also produce similar reflectivity. The shear wave properties and reflectivity of mylonites from the Brevard fault zone have been determined using measured shear velocities as a function of confining pressure. The measured shear wave velocities are strongly influenced by mineralogy, especially quartz and oriented micas. The strong oriented fabric of Brevard mylonites creates seismic anisotropy, which, for nonnormal incident propagation produces significant shear wave splitting. A wide range of *Vp/Vs* ratios within the Brevard fault zone originates from a complex combination of composition and anisotropy, making lithology determination difficult. The shear wave reflectivity of the Brevard fault zone was derived from one-dimensional normal incidence modeling of detailed geologic fault zone models. The shear wave reflectivity of the Brevard fault zone, which originates from fine compositional layering, is moderate and can be directly correlated with individual geologic formations. Within the fault zone variable shear wave reflectivity, both horizontally and vertically, originates from geologic heterogeneity. The modeled shear wave reflectivity also depends on frequency. Frequencies below 20 Hz will resolve boundary structure, while higher frequencies image detailed geologic features within the fault zone.

INTRODUCTION

Seismic reflection studies over the past 20 years have led to an improved understanding of major crustal fault zones. To date these studies have focused on compressional wave structure, [e.g., *Smithson*, 1979; *Cook et al.*, 1981; *Matthews and Cheadle*, 1986; *McCarthy*, 1986]. Seismic energy also propagates as shear waves, yet very little research has addressed fault zone shear wave reflection structure. Shear wave reflectors have been observed in the lower crust on seismic sections across northern England [*Ward and Warner*, 1989] and the former USSR [*Alekseev et al.*, 1988]. *Goodwin et al.* [1989] distinguished reflector origin by comparing phase and amplitude of both compressional and shear wave arrivals. These initial shear wave studies suggest that major fault zones may have significant observable shear wave reflectivity.

The following questions are paramount to understanding fault zone shear wave reflectivity: To what extent are fault zones reflective to shear wave energy? For example, do shear wave reflections show the same high amplitudes that are often observed in compressional wave reflection profiles? If fault zone mylonites are reflective to shear energy, what is the origin of the reflectivity? How will frequency, depth, and incidence angle affect the shear wave reflectivity?

This study addresses the shear wave reflectivity of a fault zone by using laboratory-measured shear wave velocities and densities of mylonite samples from the Brevard fault zone in the southeastern United States to calculate synthetic reflection seismograms. The studied samples come from a continuous drill core, which penetrated a depth of 300 m. Compressional wave reflectivity of this drill core section was previously investigated by *Christensen and Szymanski* [1988], who showed significant compressional wave reflectivity due to compositional layering, anisotropy, and constructive interference of seismic energy. The following analysis of shear wave properties of rocks from the Brevard fault zone provides information on shear wave reflection structure within fault zone mylonites and correlates this structure with compressional results [*Christensen and Szymanski*, 1988].

Paper number 92JB02275.
0148-0227/93/92JB-02275$05.00

GEOLOGIC SETTING

The Brevard fault represents a kilometer-wide mylonitic zone which stretches 725 km from North Carolina southeast to Alabama (Figure 1a). The linear trace of the Brevard fault structurally divides two crystalline provinces of the Southern Appalachians-the Blue Ridge to the northwest and the Inner Piedmont to the southeast. The Brevard zone splays at its southern and northern ends where its cataclastic features are less pronounced. *Keith* [1905] first described in detail the mylonites near Brevard, North Carolina as a kilometer wide zone of intensely sheared, meta-sedimentary and meta-volcanic rocks. The phyllonites of the Brevard show two stages of metamorphism-a garnet amphibolite phase and a more dominant retrograde greenschist phase [*Hatcher*, 1970; *Roper and Justus*, 1973]. Intense shearing and metamorphism have produced a strong foliation which strikes subparallel to the fault trace and dips shallowly to the southeast.

The complex deformation of the Brevard fault zone places the upper amphibolite metavolcanics and intruded gneisses of the Inner Piedmont upon the greenschist to upper amphibolite meta-sedimentary and basement rocks of the Blue Ridge [*Jonas*, 1932; *White*, 1950; *Reed and Bryant*, 1964; *Hatcher*, 1968, 1971]. *Clark et al.* [1978] investigated the subsurface geometry of the fault by producing seismic profiles 1 km and 0.6 km in length. These sections showed two shallow, high amplitude dipping reflectors, which were interpreted as the top and base of the Brevard Fault zone, giving the zone a thickness of approximately 0.3 seconds of two way travel time (~0.9 km). Later studies by Continental Consortium for Reflection Profiling (COCORP) across the Brevard [*Cook et al.*, 1981, 1983] imaged much deeper than *Clark et al.* [1978] but did not record the subtle features in the upper crust. On the COCORP records the Brevard fault zone appears as a rather incoherent package of reflectors (~0.6 km

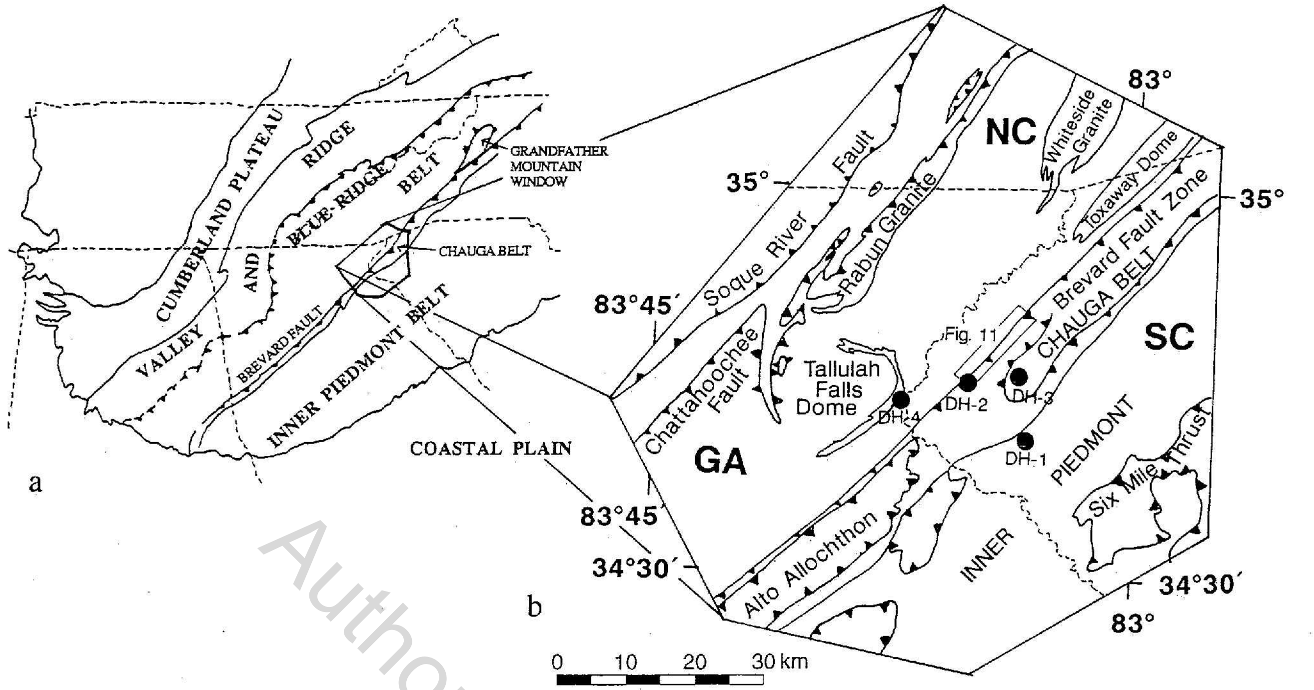

Fig. 1. (a) Index map showing the physiographic provinces of the Southern Appalachians, and the location and lateral extent of the Brevard fault zone. (b) Map showing locations of ADCOH drill core holes (DH-1 - DH-4) and major structural features (modified from *Hatcher et al.* [1987]).

thick), which soles at a depth of ~ 9 km, merging with a series of strong, horizontal layered reflectors approximately 1 km thick. More recently, a high resolution survey across the Brevard fault conducted as part of a site survey for Appalachian Ultra Deep Core Hole (ADCOH) [*Coruh et al.*, 1987; *Hatcher et al.*, 1987] imaged the reflectors of the Brevard fault zone splaying from a major decollement at 6 km depth. The decollement continued to the northwest beneath the Blue Ridge as part of duplex and imbricated structures. Recent reprocessing of the ADCOH seismic data has confirmed the original duplex structure by showing that all the major faults in the Blue Ridge - Inner Piedmont crustal block, including the Brevard fault zone, sole in the master Blue Ridge decollement [*Hubbard et al.*, 1991].

The ADCOH survey explored a 8600 km^2 area in the southern Appalachians for a possible location to drill a 10 to 11 km deep hole into the autochthonous North American basement and its deformed Paleozoic platform sedimentary rocks [*Williams et al.*, 1987; *Hatcher*, 1987]. The ADCOH survey included surface geologic mapping, seismic reflection studies, and shallow drilling. The four drill holes shown in (Figure 1b) were selected to provide information on the drilling characteristics of the different crystalline terranes in the area and to allow standard logging experiments to be performed in the holes. One hole (DH-2) located within the Brevard fault zone penetrated 300m of fault zone mylonites with nearly 100% recovery. The core's continuous and unweathered nature creates an ideal rock section to study possible shear wave reflectivity in fault zones.

The rocks from the Brevard drill core are micaceous quartzofeldspathic mylonitic gneisses and schists. A complete lithologic log compiled from visual and thin section observations divided the Brevard rocks into three lithologic units- the Poor Mountain formation, the Chauga River formation, and the Henderson Gneiss [*Williams et al.*, 1987]. The Poor Mountain formation occurring at the top of the core consists of fine recrystallized phyllonites (Figure 2), which have been thrust over a

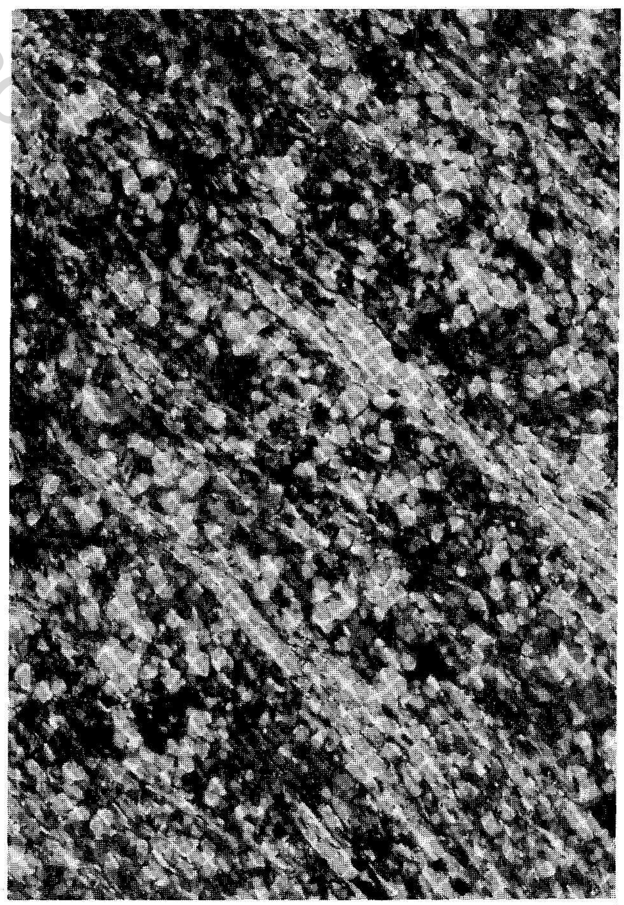

Fig. 2. Photomicrograph of a Brevard-Poor Mountain Phyllonite from 20.3m depth showing recrystallization texture and preferred mica orientation. Width of photo equals 2.2 mm.

sliver of Henderson Gneiss. The Henderson Gneiss appears twice in the drill core, once as a 40m section below the Poor Mountain formation and again as the lower 140 meters of the core. The Henderson Gneiss is a mica, quartz, feldspar augen gneiss (Figure 3) with a relatively uniform grain size and composition. The Chauga River formation divides the two sections of Henderson

Fig. 3. Photomicrograph of Henderson gneiss, from 191.2m depth showing feldspar augens and preferred mica orientation. Width of photo equals 2.2 mm.

Gneiss and shows large variations in composition and grain size, including two phyllitic members and a carbonate member. Chemical analyses presented by *Christensen and Szymanski* [1988], as well as modal estimates (Table 1), confirm this compositional heterogeneity.

Physical Properties

The compressional wave reflectivity study of the Brevard mylonites by *Christensen and Szymanski* [1988] used 34 samples from the Brevard fault zone core spaced at actual geological intervals averaging 10 m. Shear wave velocities were measured on these 34 samples plus 9 new samples. These velocities will be used later to calculate the shear wave reflectivity. The additional samples were selected at intervals showing major compositional variability. To investigate shear wave anisotropy, three perpendicular minicores [*Christensen and Szymanski*, 1988, Figure 4], 2.5 cm in diameter and 4-6 cm in length, were prepared for velocity measurements. The axes of the A-cores were oriented normal to the foliations. The B and C cores were cut parallel to the foliations and perpendicular to one another, with the axes of the B cores parallel to the lineations.

The bulk density of each minicore was calculated from its weight and dimensions before jacketing. The velocity measurement preparations include jacketing the cores in copper, attaching brass tabs on the core ends, and inserting this assembly in rubber tubing to prevent oil saturation during the high pressure runs [*Christensen*, 1985]. After jacketing, shear wave velocities were measured using a pulse transmission technique [*Birch*, 1960] to hydrostatic confining pressures of 600 MPa (equivalent to crustal depths of approximately 20 km). The combination of transducers used for shear measurements were AC quartz, as a sending transducer because of its low longitudinal component, and lead zirconate titanate (shear mode), as a receiver because of its large electrical output for unit displacement. Shear wave velocities often are more difficult to measure than compressional wave velocities as a result of the relatively low output of shear transducers, the interference by the compressional energy with the shear wave first arrival, and the rock's anisotropic effect on the shear energy, which often produces shear wave splitting. Each problem requires special consideration. To improve the low output of the shear signal, an amplifier enhances the signal and the brass tabs added during jacketing increase the conductance at the core ends. Using a sample length between 4 and 6 cm eliminates the compressional wave energy interference. The anisotropic effects are taken into account by careful orientation of the transducer vibration direction with rock structure.

The measured shear velocities for the A cores, at various pressures, and their densities, at atmospheric pressure, are displayed as a function of depth in Figure 4. The shear velocities were measured to high pressures for two reasons. First, the typical velocity versus pressure curve for crystalline rocks generally shows a rapid increase in velocity below 200 MPa, which is related to the closing of cracks [*Birch*, 1960]. This applies for both compressional wave velocities [*Christensen and Szymanski*, 1988] and shear wave velocities (Figure 5) of the Brevard mylonites. Above 200 MPa, velocity increases linearly with increasing pressure, reflecting the influence of mineralogy on velocity. Second, it is clear from the textures and mineralogies of the Brevard fault mylonites that they originated at intermediate crustal depths corresponding to pressures from 300 MPa to perhaps as high as 600 MPa. Thus, velocities measured to these pressures will be useful in interpreting fault zone shear reflections from the deeper crust, as well as at shallow depths where the fault zone extends to the surface.

Compositional Influences

Compositional influences on the shear properties are shown in Figure 6. The single crystal averaging techniques used to obtain the monomineralic velocities have been discussed by *Birch* [1961] and *Christensen* [1965, 1966, 1982]. The mylonite velocities fall within a field defined by quartz, feldspar (microcline and oligoclase), and the phyllosilicates, chlorite and biotite. Quartz has an extremely high shear velocity for its relatively low density [*Christensen*, 1966] (Figure 6). Thus for the Brevard mylonites, quartz will produce an increase in shear velocity as the quartz content increases. This relationship has been shown to cause the negative linear relationship between shear velocity and density in granulites [*Christensen and Fountain*, 1975] and siliceous limestones [*Wilkens et al.*, 1984].

In addition to quartz and feldspar, the Brevard mylonites also contain variable amounts of biotite and chlorite. While there is no single crystal information on chlorite, *Christensen and Wilkens* [1982] found a chlorite aggregate to have a high density and a low shear velocity similar to biotite. Thus for the Brevard mylonites,

TABLE 1. A-Core Velocities (Va) and Anisotropies (A)

Sample Depth, m	Mineralogy	Velocities, km/s Anisotropies, %	Pressure, MPa					
			50	100	200	400	600	1000
29.0		Va	3.091	3.149	3.208	3.268	3.304	3.351
	(52%Q, 40%M)	A	20.7	20.0	19.4	18.7	18.4	17.9
34.7		Va	3.336	3.391	3.447	3.489	3.507	3.526
	(45%Q, 30%M, 15%C, 5%Cl)	A	15.0	13.7	13.0	12.8	12.7	12.6
43.6		Va	3.373	3.494	3.567	3.604	3.623	3.647
	(25%Q, 57%F, 15%M)	A	7.1	5.6	4.7	4.4	3.9	3.4
84.4		Va	3.041	3.138	3.229	3.29	3.315	3.343
	(25%Q, 35%M, 20%Cl, 12%G)	A	31.2	28.0	25.2	23.6	23.0	22.3
122.0		Va	3.412	3.454	3.489	3.518	3.534	3.555
	(50%Q, 25%M,10%F, 10%C)	A	13.1	12.8	12.4	12.1	11.8	11.6
126.8		Va	3.347	3.389	3.417	3.433	3.441	3.451
	(60%Q, 15%M, 10%C, 10%Cl)	A	14.6	14.3	14.0	13.8	13.7	13.6
144.8		Va	3.397	3.423	3.448	3.471	3.484	3.500
	(50%Q, 10%M,10%F, 20%Cl,	A	11.8	11.6	11.1	10.9	10.8	10.8
167.9		Va	3.245	3.274	3.308	3.345	3.366	3.390
	(25%Q, 10%M, 40%F, 20%Cl)	A	13.5	13.3	13.0	12.5	12.2	11.8
170.1		Va	3.375	3.451	3.503	3.543	3.565	3.594
	(35%Q, 20%M,30%F, 20%C)	A	11.0	9.9	9.2	8.9	8.8	8.6
212.5		Va	3.458	3.5	3.542	3.588	3.618	3.656
	(25%Q, 15%M, 40%F,15%Cl)	A	7.5	7.5	7.1	6.5	6.1	5.5
244.8		Va	3.421	3.487	3.561	3.654	3.714	3.793
	(30%Q, 15%M,15%F, 10%Cl,	A	3.5	5.3	6.2	6.4	6.4	6.4
274.9		Va	3.384	3.507	3.566	3.599	3.618	3.641
	(35%Q, 20%M, 35%F)	A	9.5	8.6	8.1	7.7	7.5	7.3
303.9		Va	3.229	3.360	3.404	3.426	3.438	3.454
	(30%Q, 22%M, 20%F, 8%Cl)	A	8.4	7.0	6.6	6.4	6.3	6.1

Q, quartz; M, mica (muscovite & biotite); F, feldspar (K-spar & plagiclase); C, calcite; Cl, chlorite; G, garnet; E, epidote

an increase in biotite and chlorite produces a shear velocity decrease and a density increase. This effect is magnified during metamorphism when the phyllosilicates become oriented, with their slow axes normal to the foliation, producing significant anisotropy. Finally, the shear velocities of the Brevard fault zone are spread out by varying amounts of feldspar, calcite, and muscovite, which have low shear velocities associated with low densities. Thus, the shear velocities of the Brevard fault zone rocks are governed by mineral composition and anisotropy, with particular emphasis on quartz content and mica orientation.

Shear Wave Splitting

Shear wave splitting occurs when an incident wave enters an anisotropic medium and divides into two orthogonal components, which travel at different velocities. The velocity difference produces a time separation which, over a sufficient distance, gives two clearly distinguishable shear wave arrivals [*Christensen*, 1984, Figure 11]. Shear wave splitting is generally attributed to preferred mineral orientation [*Christensen*, 1966] and/or aligned fractures [*Crampin*, 1985].

Christensen and Szymanski [1988] have shown that the strong foliation, due to mineral orientation, of the Brevard mylonites produces varying amounts of compressional wave anisotropy, which influenced the reflectivity. To determine the anisotropy and its effect on shear waves, we selected a few samples for detailed velocity measurements. The structure of many foliated metamorphic rocks can be simplified by assuming that the strong foliation produces a transversely isotropic symmetry throughout the fault zone [*Christensen*, 1965, 1966]. This symmetry was verified by determining the complete elastic properties of a Brevard mylonite. In a transversely isotropic medium propagation along the A core produces no variation in shear velocity with vibration direction, but for propagation along a B or C core, shear velocities show a maximum variation between vibrating parallel to the foliation and vibrating perpendicular to the foliation. Figure 7 shows the significant velocity differences for selected B cores. One observes the highest velocities for shear waves propagating and vibrating parallel to foliation.

The shear wave anisotropy, defined as the difference between the maximum and minimum velocities in a sample expressed as a percentage of the mean [*Birch*, 1960], is given in Table 1 with A core velocities, as a function of pressure. Mineral and crack alignments are the primary causes of velocity anisotropy. Crack anisotropy is minimized by using pressures above 200 MPa [e.g., *Siegesmund et al.*, 1991]. Mineral induced shear wave splitting in a rock will vary depending on the elastic anisotropy of the mineral constituents and the degree of their preferred orientation. The mineral orientation of the Brevard mylonites produces variable amounts of compressional anisotropy [*Christensen and Szymanski*,

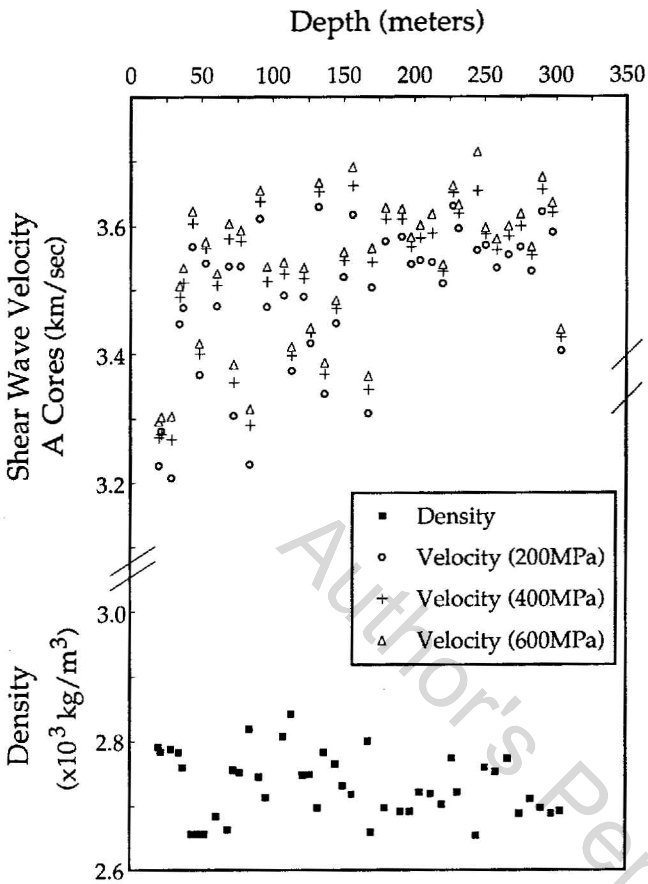

Fig. 4. Measured A core shear velocities at 200, 400, and 600 MPa and densities at atmospheric pressure plotted as a function of depth.

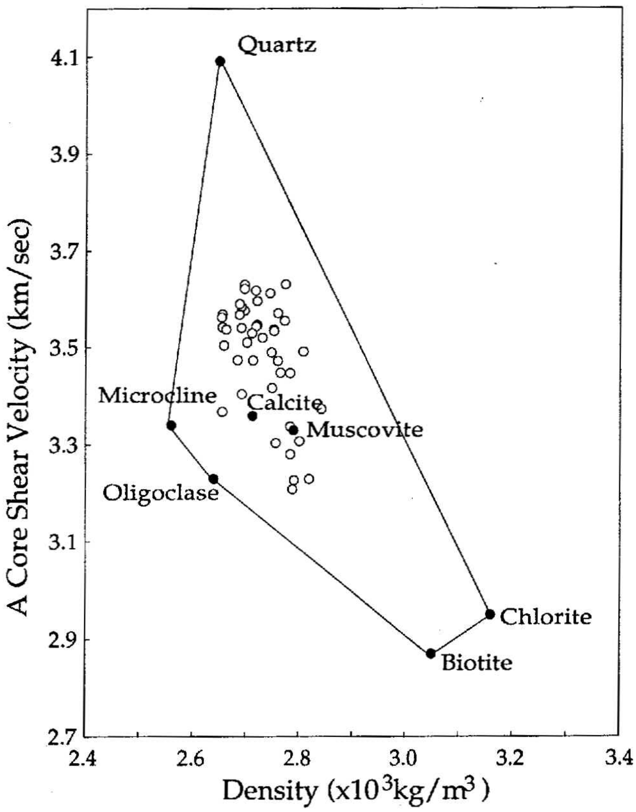

Fig. 6. A plot showing A core shear velocities versus density at 200 MPa with densities and Voigt-Reuss-Hill velocities for the major minerals comprising the Brevard mylonites [*Christensen* 1965, 1966, 1982].

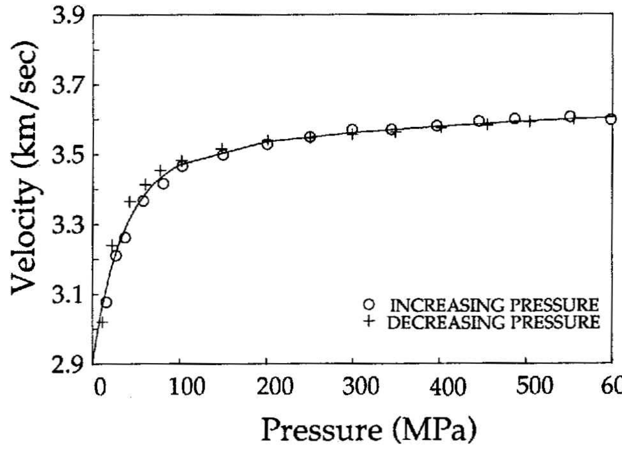

Fig. 5. Shear wave velocities presented as a function of pressure for the A core at 69.9 m depth.

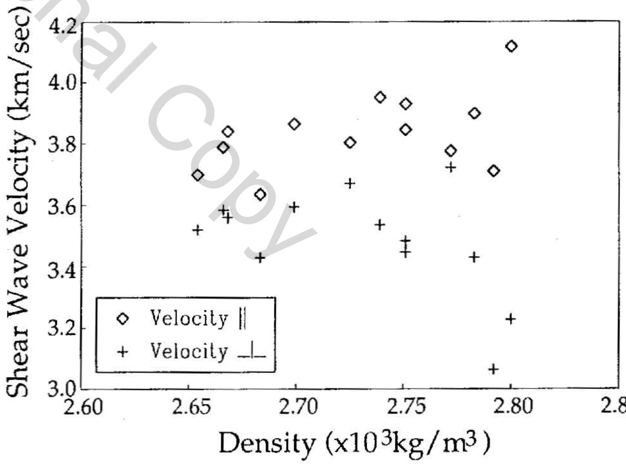

Fig. 7. Shear wave splitting as illustrated by selected B core shear velocities at 200 MPa versus density for vibration direction parallel and perpendicular to the foliation.

1988] and the shear wave velocities also show similar variations in anisotropies, which correlate well with mica content (Figure 8).

The velocity differences shown in Figure 7 allow travel time splitting predictions for shear field surveys. Using the velocities from Figure 7, calculations of shear wave splitting effects for a 10 m layer produces travel time differences ranging from 0.001 to 0.003 seconds. Thus, the maximum observed travel time difference through a 1-km-thick fault zone is 0.30 seconds. This difference would be clearly distinguishable on recorded traces for a horizontal fault slab with vertical foliation. Most major thrust faults however, have subhorizontal foliations giving rise to minimum shear wave splitting for normal incidence.

Velocity -Density and Vp/Vs Relationships

The need for additional subsurface information has fostered an interest in shear wave properties of various rock types. A combination of compressional and shear wave seismic profiles allows lithologic characteristics to be estimated from seismic properties. The following discussion compares the compressional

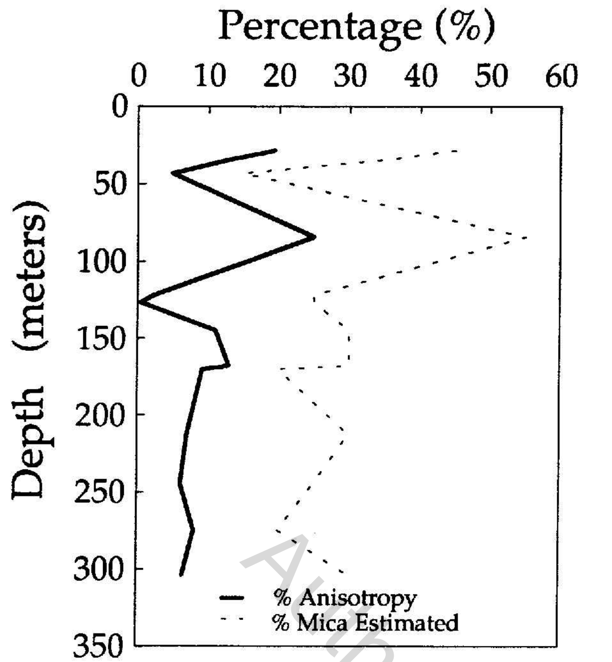

Fig. 8. Percent shear wave anisotropy and mica content plotted as a function of depth.

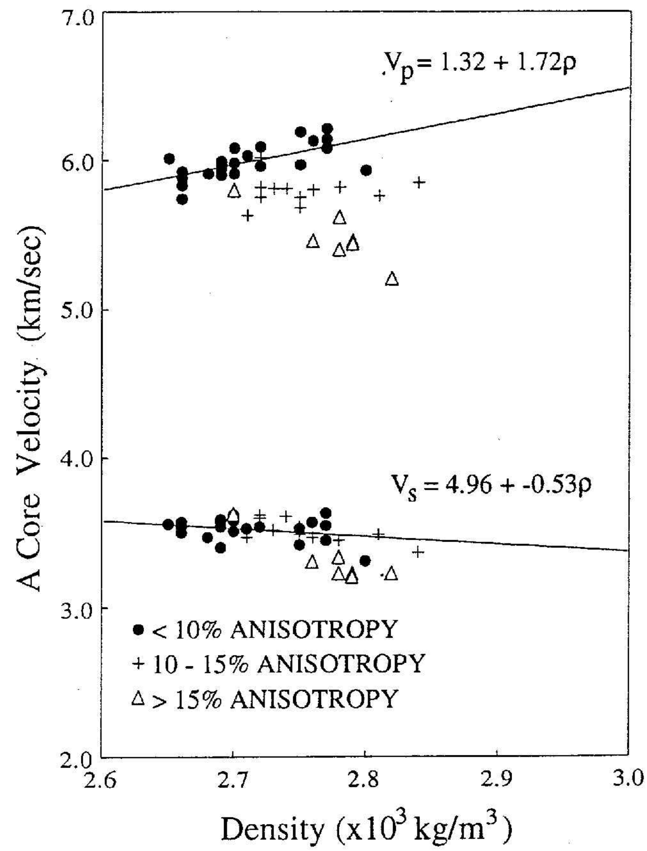

Fig. 9. A core compressional and shear velocities at 200 MPa versus density, as a function of anisotropy. The solid lines represent the best fit linear regression for samples with anisotropy below 10%.

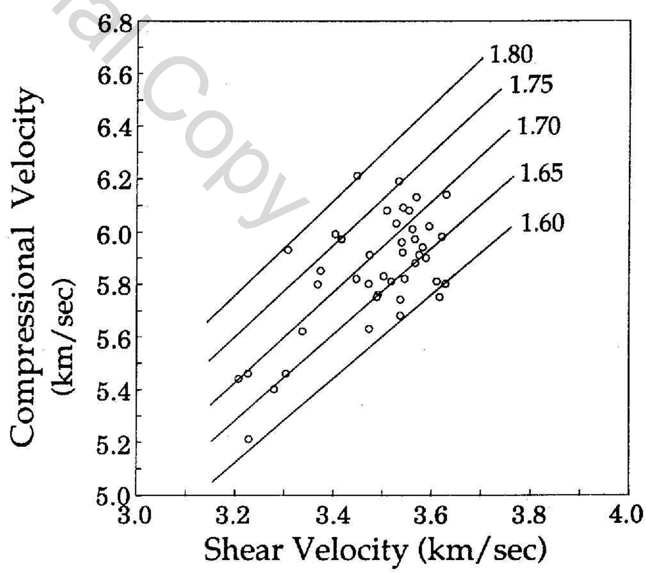

Fig. 10. Compressional wave velocities versus shear wave velocities. Solid lines represent lines of constant *Vp/Vs* ratios.

wave [*Christensen and Szymanski*, 1988] and shear wave properties of the Brevard mylonites through an examination of the velocity and density relationships.

Since modeling and reflection profiles for regions with semi-horizontal layering relate primarily to A core velocities, the A core velocities have been selected for this discussion. In Figure 9 compressional and shear wave velocities at 200 MPa are plotted as a function of density and anisotropy. The linear regression for the compressional velocities, $Vp = 1.724\rho + 1.318$, for mylonites with low anisotropy shows the expected increase in velocity with density increases [*Birch*, 1961], yet as the anisotropy increases A core velocities decrease. This decrease corresponds to an increased orientation of the phyllosilicate minerals' slow velocity direction with the A Core orientation, during deformation. The observed negative slope in the linear regression for the shear velocities versus density, $Vs = -0.529\rho + 4.958$, is likely related to decreasing quartz content with increasing density. Quartz has a higher shear velocity relative to feldspars and micas. Although less pronounced than the decrease in compressional velocities, shear velocities also exhibit a decrease with increasing anisotropy.

The relationship between compressional and shear velocities, known as the *Vp/Vs* ratio, is often used to estimate the lithology of subsurface rocks from sonic logs or seismic reflection profiles [*McCormack et al.*, 1984; *Wilkens et al.*, 1984]. The wide range of *Vp/Vs* values for the Brevard mylonites originates from variable mineral properties, but anisotropy causes complications in any estimation of lithology from seismic techniques. This wide range of compressional and shear velocities in the Brevard mylonites is shown in Figure 10. Also plotted are lines of constant *Vp/Vs* ratio. The samples with low compressional and shear velocities have high anisotropy due to the strong preferred orientation of mica. Those samples with *Vp/Vs* ratios below 1.70 have relatively high quartz content. Finally, the samples with *Vp/Vs* ratios higher than 1.75 contain abundant garnet or epidote.

This examination of the seismic properties of the Brevard mylonites revealed the importance of composition and mineral alignment on their recorded seismic velocities. These influences should also play a critical role in producing reflectivity within the fault zone. *Christensen and Szymanski* [1988] have already shown that, for compressional waves, reflectivity originates from compositional and anisotropy variations of the fault zone mylonites. The shear wave reflectivity modeling which follows also concentrates on compositional and anisotropic origins.

Shear Wave Reflectivity

Predicting shear wave reflectivity of the Brevard fault zone will show the usefulness of shear wave reflection surveys in imaging major fault zones and defining subsurface lithologies within fault zones. The following discussion addresses the origin of shear wave reflectivity by creating synthetic seismograms from geological fault models and measured velocities and densities. The reflectivity derived from these models will show both the lateral and vertical variation in the reflective nature of the Brevard fault. Finally, this shear wave reflectivity is compared to the compressional reflectivity to determine possible relationships between seismic mode, lithology, and reflectivity.

Geologic Model

Modeling reflectivity requires knowledge of both the detailed fault stratigraphy and the corresponding velocity characteristics of each lithology. The geology of the Brevard fault zone shows a great deal of variability along strike (Figure 11) making it difficult to create a generalized stratigraphic section of the fault zone. Therefore, to investigate possible lateral heterogeneity three stratigraphic sections (Figure 12) were created from the geologic maps (Figure 11) of *Horton* [1982] and *Edelman et al.* [1987]. Section A (Figure 12a) contains the DH-2 drillhole section as the top portion of the stratigraphic column.

For complete modeling of the fault zone, it is important to include the lithologies above and below the fault zone. Above the fault zone, *Griffins'* [1974] detailed mapping of the Inner Piedmont suggests three possible descriptions of the hanging wall geology. These possibilities are a highly reflective Inner Piedmont section, a seismically transparent zone produced by variable anisotropy due to severe deformation, or a thick section of Henderson Gneiss. To simplify modeling, a 100 meter slab of Henderson gneiss was placed above the fault zone. Below the fault zone lies the Tallulah Falls formation (Figure 11), which is represented by the first 100 meters of drillhole DH-4.

An impedance model for each stratigraphic section was created from measured velocities densities and thicknesses in order to determine reflectivity. Section B (Figure 12b) has a 100 meter thick section of the Upper Phyllite member in the Chauga River formation; to create this lithologic unit, the upper phyllite samples from DH-2 were randomly sequenced to a total thickness of a hundred meters. This sequencing was repeated for every unit in the three sections, with the exception of Section A where the DH-2 section was left intact. Special care was taken to maintain the

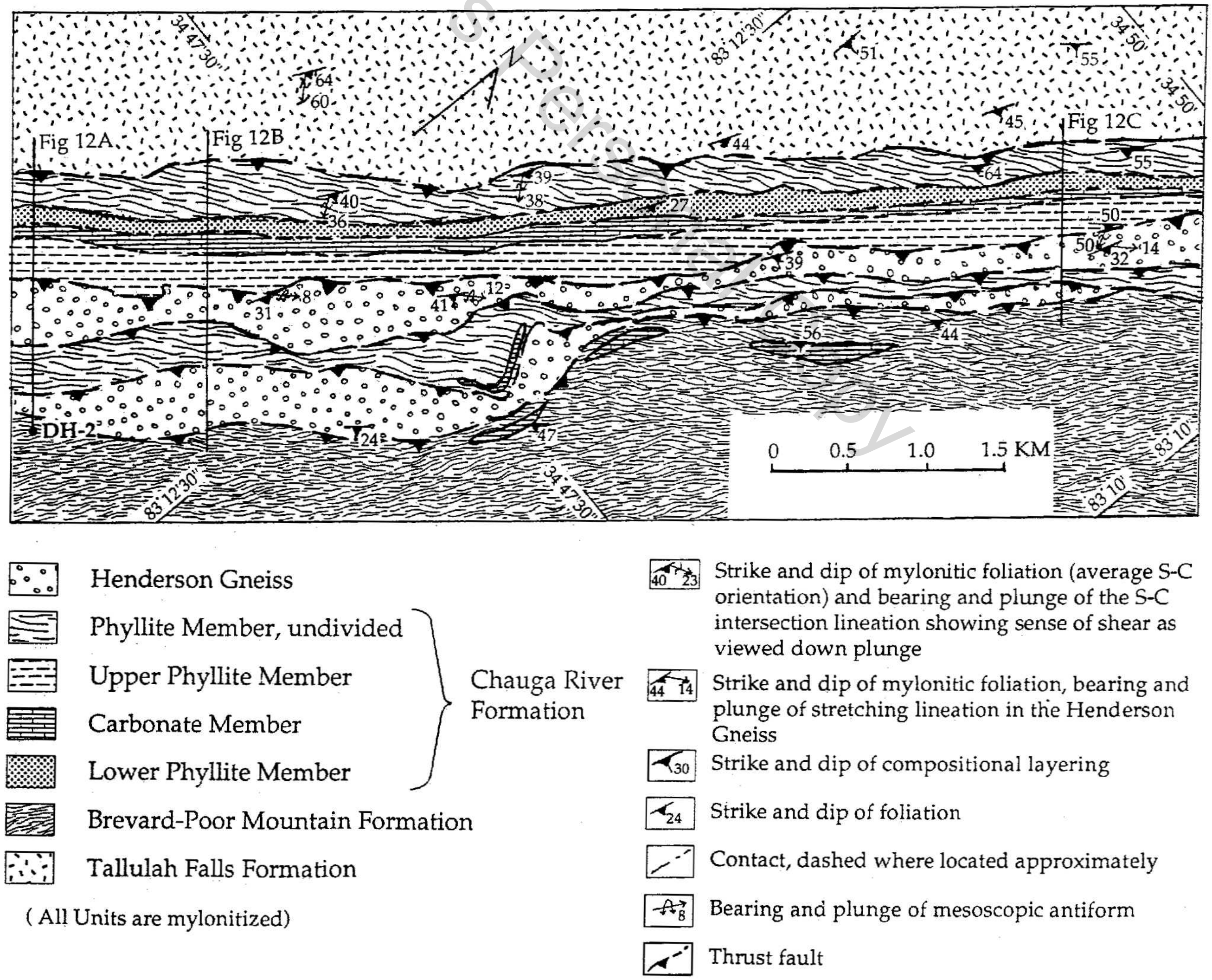

Fig. 11. Geological map detailing the Brevard fault zone around DH-2 (modified from *Horton* [1982] and *Edelman et al.* [1987]). Also shown are locations of the three cross-section lines of Figure 12. See Figure 1 for location.

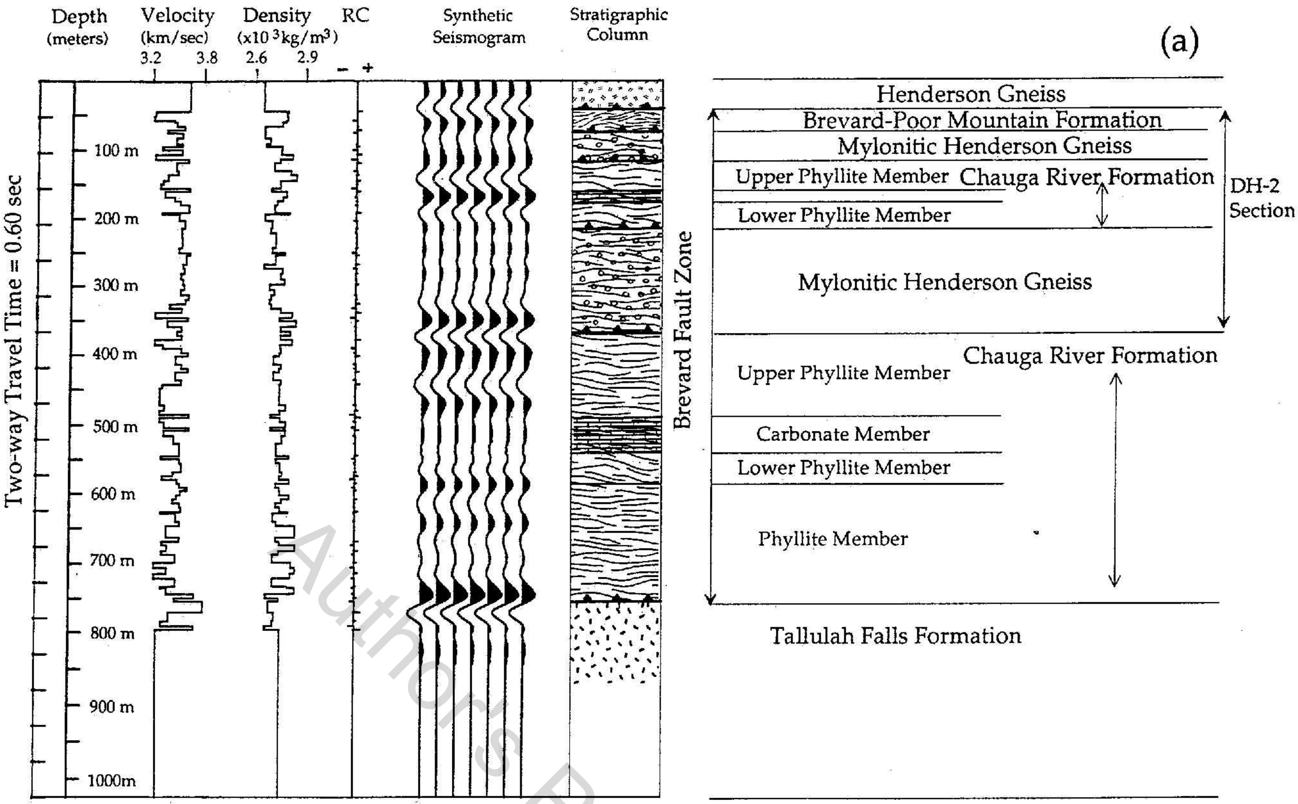

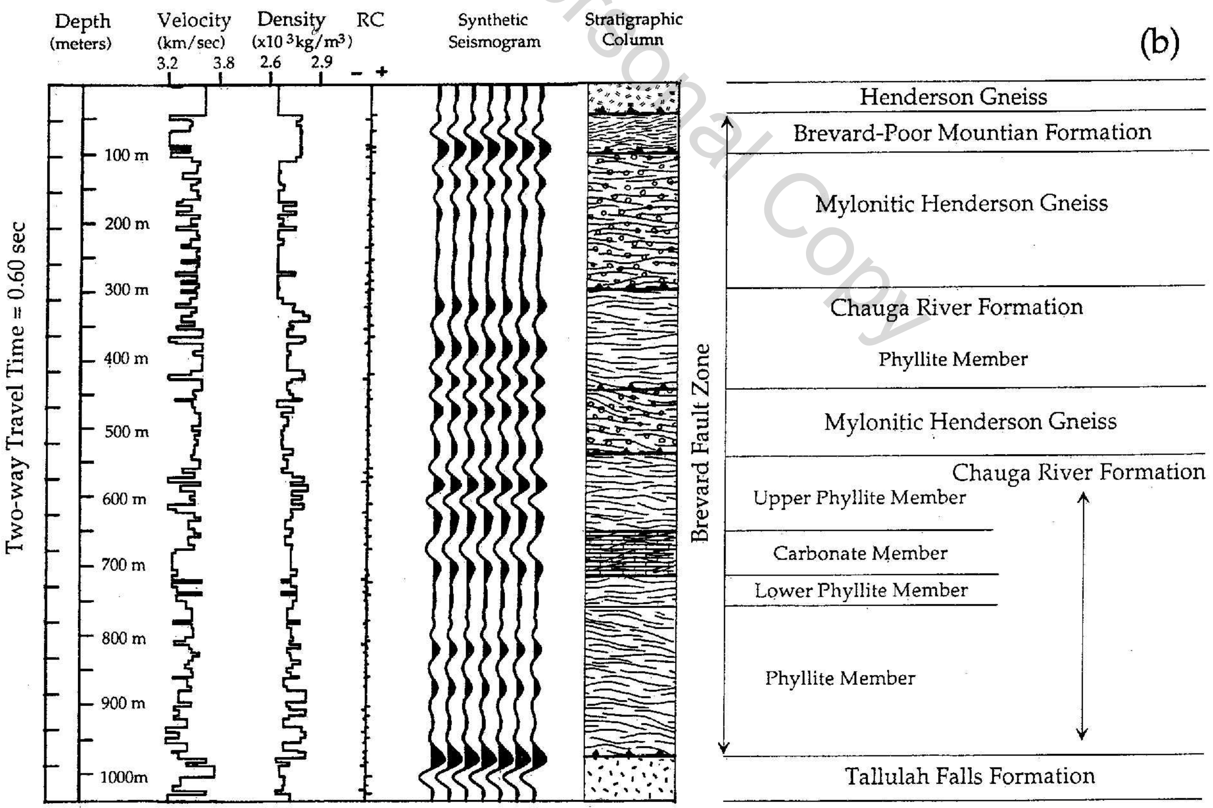

Fig. 12. Shear wave reflectivity at 200 MPa calculated for each of the three stratigraphic sections through the Brevard fault zone. The vertical axis is total two-way travel time equal to 0.60 s and depth equal to 1000 m. Also plotted are the velocity, density, and stratigraphic models. (a) Stratigraphic section containing the measured DH-2 section as the upper third of the stratigraphy. (b) and (c) Stratigraphic sections showing the fault's variability along strike. An average dip of ~35 degrees was corrected for when constructing these normal stratigraphic sections.

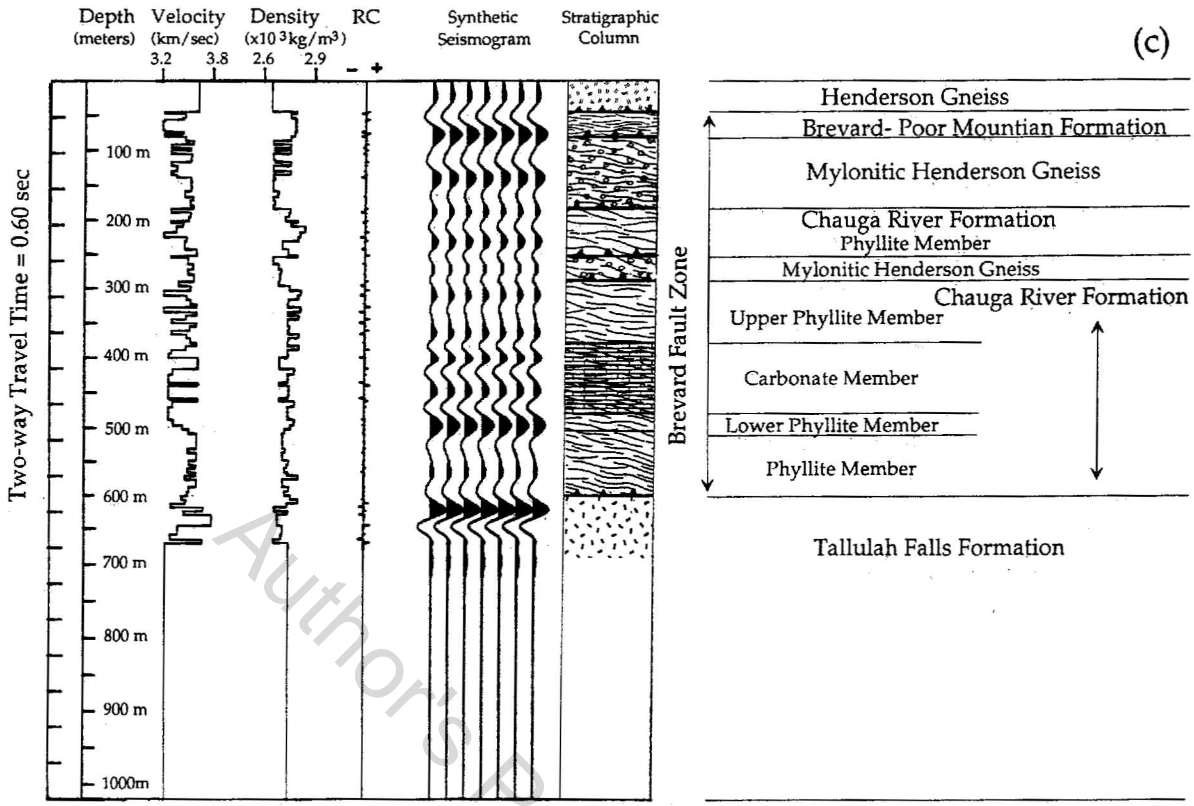

Fig. 12. (continued)

velocity and density relationships at each contact between units while constructing the models. The randomization of samples was used to prevent imaginary sequence boundary reflections. To complete the fault zone models, additional measured velocities and densities were used for the lithologies lying above and below the fault zone.

Modeling Technique

One-dimensional modeling describing plane wave propagation in layered media has been developed and used extensively in reflection seismology [e.g., *Weunschel*, 1960; *Claerbout*, 1968; *Robinson and Treitel*, 1977]. These modeling techniques present mathematical representations of a normal incident acoustic wave propagating through a homogeneous layered media by describing the reflected and transmitted response of an input signal. The simple modeling of shear wave reflectivity requires maintaining normal incidence. Therefore all the velocities used in the impedance models were the normal A core velocities. The mathematical representation of the shear wave propagation in a homogeneous media follows the acoustic algorithm maintaining both displacement and stress boundary conditions giving a reflection coefficient of $RC = (Z_n - Z_{n+1})/(Z_n + Z_{n+1})$, where Z_n represents the impedance (velocity times density) of the nth layer [*Aki and Richards*, 1980]. This varies from the acoustic model only by an inverse sign in the reflection coefficients, which produces a 180 phase shift on the shear wave seismogram. Although the synthetic seismogram considers transmission losses at interfaces, no attempt is made to account for dispersion, geometrical spreading, attenuation, or multiples.

Reflectivity Results

Figures 12a-12c show the calculated reflectivity for each of the three stratigraphic sections at 200 MPa with a median frequency of 25Hz. Each section is plotted both as a function of two-way travel time equal to 0.60 seconds and depth equal ~1000 m. Because the sections are presented in equal time and depth, shorter sections appear non-reflective at depth, (Figures 12a and 12c). The velocity and density models are also plotted with depth. The reflection coefficient series (RC) is shown with spikes to the right representing positive shear impedance contrasts. Finally, the resulting synthetic seismogram is shown seven times to simulate a segment of a zero-offset two-dimensional seismic record. The stratigraphic column is placed next to the calculated synthetic seismogram to correlate reflectivity and composition. For amplitude reference, the largest reflector observed represents an interface with a reflection coefficient of ~ 0.05.

All three reflectivity models (Figures 12a-12c) show moderate reflectivity, with relatively strong reflectors at the fault boundaries. In Figures 12a and 12b, zones lacking reflectivity generally correlate to units of Henderson Gneiss, while the more reflective zones are associated with the Chauga River Formation. This correlation is supported by a comparison of internal reflection coefficients for both formations (Figure 13). Figure 13 was created by calculating reflection coefficients of internal interfaces within each formation of the DH-2 section and plotting them as a function of occurrence. From this, it is apparent that the stronger reflection coefficients (RC > 0.03) are generally related to the Chauga River formation, while a majority of the weak reflectors (RC < 0.01) are found in the Henderson Gneiss, confirming that compositional variations cause shear wave reflectivity.

Many compressional wave studies of thin-layered models have shown that constructive and destructive interference of the reflected seismic energy influences the observed reflectivity [*Widess*, 1973; *Ruter and Schepers*, 1978; *Schoenberger and Levin*, 1979; *Hurich and Smithson*, 1987; *Christensen and Szymanski*, 1988; *Wang et al.*, 1989; *Christensen*, 1989]. The

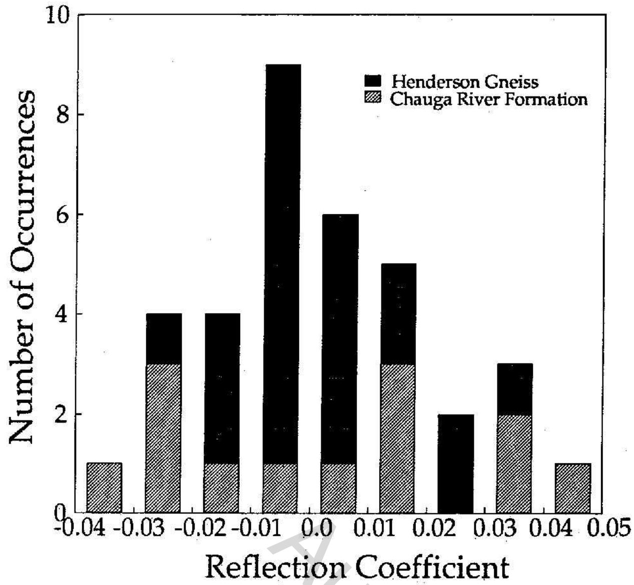

Fig. 13. A comparison of the internal reflection coefficients in the Henderson Gneiss formation and the Chauga River formation at 200 MPa.

relatively strong reflectivity in Figure 12c possibly originates from this thin bed constructive interference. The constructive interference affects the reflectivity models because there is no direct correlation between the prominent reflection coefficients and strong reflectors.

With the exception of the reflector at the base of the fault zone, the three reflectivity models contrast strongly in their reflectivity. This difference is produced by variations in geology along the fault zone. If this variation is typical within the fault zone, shear wave reflection surveys would observe discontinuous dipping reflectors. It is likely these shear wave reflectors would resemble the discontinuous reflectors already observed on the compressional profiles [*Cook et al.*, 1981, 1983; *Coruh et al.*, 1987; *Hatcher et al.*, 1987; *Hubbard et al.*, 1991]. The most prominent and continuous reflection would be observed at the base of the fault zone, providing that the geology of the Tallulah Falls formation is laterally invariant.

From the above discussion it is clear that shear wave reflectivity in the Brevard fault zone is likely to originate from a complex combination of thin layer thicknesses, compositional variations, and reflection energy interference. These factors show that the shear and compressional wave reflectivity will generally have similar origins in the Brevard fault zone. Although *Christensen and Szymanski* [1988] have shown anisotropy due to mineral orientation to play an important role in enhancing compressional wave reflectivity, anisotropy does not appear to improve shear wave reflectivity. Further research on other mylonitic fault zones is needed to better understand the reflective properties of mylonites.

Comparison of V_P and V_S Reflectivity

Comparing compressional and shear wave reflectivity presents inherent difficulties because the higher compressional velocities produce differences in two-way travel time, wavelength, and frequency. Figure 14 presents equal-depth synthetic seismograms of compressional reflectivity at 25 Hz and shear reflectivity at 25 Hz and 15.8 Hz. Each seismogram was constructed using the section A (Figure 12a) impedance model at 200 MPa as the representative section of the Brevard fault zone. The phase of the shear wave synthetic seismograms is shifted 180 to account for the inherent phase shift between the compressional and shear wave reflectivity. Figure 14 allows comparisons of reflectivity to be made in both equal wavelength and equal frequency domains.

The equal wavelength comparison of compressional reflectivity at 25 Hz and shear wave reflectivity at 15.8 Hz (Figure 14) shows a similar high amplitude basal reflector and a few dissimilar internal reflectors. The amplitude of the shear reflectivity is observed to slightly less than the compressional reflectivity. These observations suggest that constructive interference of long wavelengths in complex structural zones produces poor resolution of the internal features, but image instead, the dominate boundary structure of the fault zone.

The earlier shear wave reflectivity models of the Brevard fault zone however, suggests that using a higher frequency of 25 Hz produces more detailed reflectivity which corresponds to the internal geologic structure. The equal frequency comparison (Figure 14) shows the shear wave reflectivity having higher resolution, but lower amplitudes than the compressional reflectivity. The longer wavelength of the compressional reflectivity also smooths the reflecting interfaces, enhancing the observed difference between compressional and shear data. The higher resolution of the shear reflectivity is to be expected since shorter wavelengths image smaller features.

From the comparison of compressional and shear reflectivity, significant amplitude and imaging differences can be described. First, the smaller amplitudes in shear reflectivity can be explained by examining the absolute difference in reflection coefficients. Figure 15 was constructed by calculating the absolute reflection coefficient at each interface from Figure 12a for both shear and compressional models, then subtracting the compressional coefficients from the shear coefficients to obtain the difference as a function of depth. From the reflection coefficient difference calculation, negative values correspond to stronger compressional reflectors and zero values correspond to equivalent reflectors. Figure 15 shows the compressional reflectivity being generally stronger than shear reflectivity. The stronger compressional reflectivity is derived from the effect of anisotropy on the A core velocities (Figure 9). As noted earlier, the compressional velocities are distributed by anisotropy over a wider range of values than shear velocities. This wide range of velocities was shown by *Christensen and Szymanski* [1988] to enhance the compressional reflectivity. Anisotropy has a lesser effect on the shear wave velocity range and no observable effect on shear wave reflectivity and, therefore, produces the observed weaker shear wave reflectivity. These results suggest that a shear reflection profile across the Brevard fault zone would display fewer reflectors with a high signal-to-noise ratio. Additionally, if the reflectors dip such that foliation is not normal to the source, the shear reflectivity may be obscured by the splitting of an already weak signal.

Second, there is a significant difference in the observed reflectivity when modeled at various frequencies. These frequency variations should influence the design of coupled compressional and shear reflection surveys. Presently, compressional and shear profiles are coupled using a compressional wave bandwidth of 14 to 50 Hz, while the shear wave frequency is half the bandwidth, ranging from 4 to 25 Hz [*McCormack et al.*, 1984; *Edelmann and Helbig*, 1989; *Loyotte*, 1989]. The modeled shear wave reflectivity suggests that a shear wave field survey over the Brevard fault zone using this frequency range (4-25 Hz) would produce only a dominant shear basal reflector for comparison with the compressional profile and, thus,

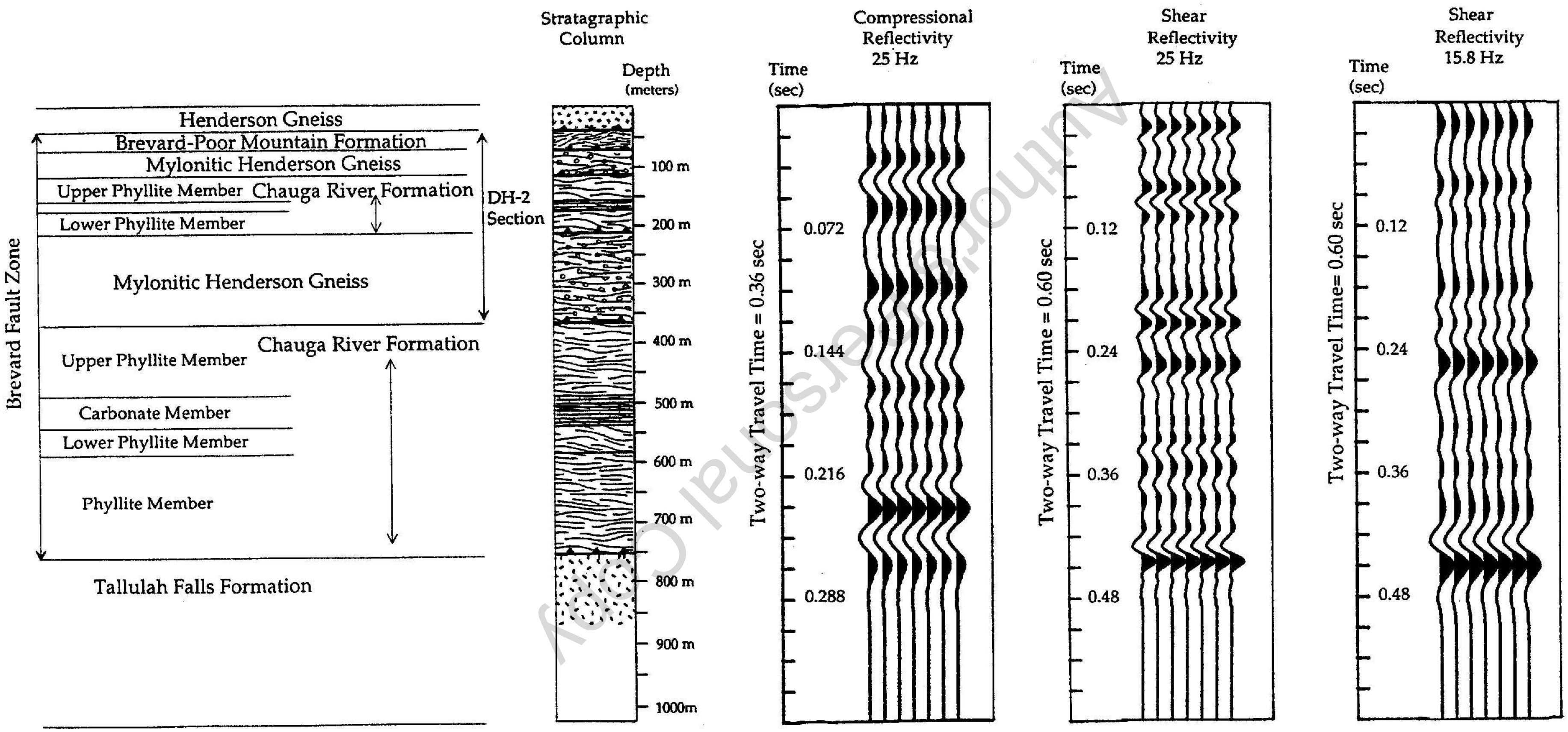

Fig. 14. A comparison of compressional and shear wave reflectivity in the Brevard fault zone at 200 MPa. Both equal wavelength and equal frequency comparisons are shown.

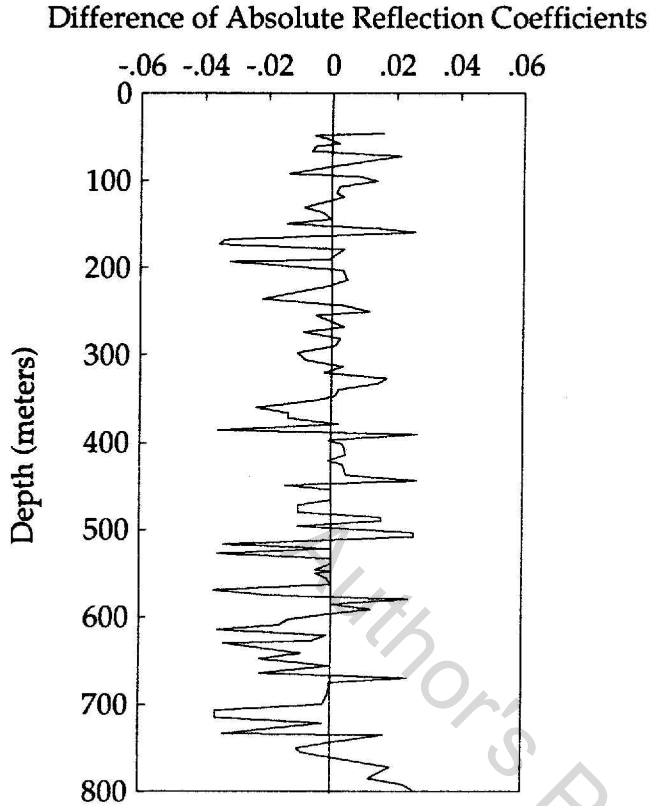

Fig. 15. The absolute difference between compressional and shear reflection coefficients of Figure 12a plotted as a function of depth. Negative values represent greater compressional coefficients than shear at an interface.

very little internal structure would be defined. A seismic line utilizing a higher-frequency bandwidth (15-35 Hz), however, would record resolvable reflections, at least at shallow depths, which define the internal geologic structure. Unfortunately, there are limitations on the useable frequency range in shear wave surveys due to attenuation of the higher frequencies and poor shear source coupling. This means the frequency range and structure geometry need to be carefully considered when studying shear wave reflectivity.

The comparison of compressional and shear reflectivity demonstrates that compressional wave reflectivity will normally be stronger than shear reflectivity. This statement does not imply that shear waves are insignificant to the subsurface study of mylonitic fault zones. Shear wave reflectivity could improve the resolution of subsurface structure and internal geology, especially at shallow depths.

Summary and Conclusions

The shear wave properties and reflectivity characteristics in a mylonite zone have been examined using measured shear velocities and densities, compositional descriptions, and one-dimensional synthetic seismogram modeling. The continuous core through a major part of the Brevard fault zone was essential to this study of the shear waves. It allowed for stratigraphic control, as well as unweathered samples for laboratory studies. Conclusions pertaining to the shear wave properties and reflectivity in the Brevard mylonite zone are as follows:

1. Shear velocities within the Brevard fault zone relate to mineralogy and mineral orientation. Within the mylonites an increase of quartz content and a decrease of anisotropy increases shear velocities normal to foliation.

2. The mineral constituents of the Brevard mylonites have a wide range of *Vp/Vs* ratios. Using these ratios to determine lithology, however, is complicated by anisotropy.

3. Shear wave splitting is minimized for propagation normal to foliation. A shift off normal incidence may effect shear wave reflectivity, because shear wave splitting will complicate field records and modeling of reflectivity.

4. The Brevard fault zone is predicted to display moderate-to-weak shear wave reflections. This is related to relatively small reflection coefficients at interfaces throughout the section.

5. The shear reflectivity in the Brevard fault zone originates from compositional layering both within and between individual formations. Enhancement of reflectivity by constructive interference should be common in regions with many thin layers.

6. The degree of lateral and vertical variation in the geology along the Brevard Fault zone will dictate the continuity of the observed reflectivity. Changes in thickness, composition, and stratigraphic relationships throughout the fault zone will produce discontinuous reflectors.

7. The anisotropic fabric of the Brevard mylonites affects shear wave velocities and will produce shear wave splitting for nonnormal incident propagation. Anisotropy does not strongly enhance the fault zone's internal shear wave reflectivity.

8. The stronger compressional reflectivity is related to a wide compressional wave velocity distribution, which creates stronger reflection coefficients.

Many major fault zones like the Brevard have been portrayed on compressional reflection profiles as semi-continuous, dipping high amplitude reflectors. Some examples are the Outer Hebrides thrust and the Moines thrust in Scotland [*Matthews and Cheadle*, 1986], the Wind River thrust in Wyoming [*Smithson et al.*, 1979], and the Snake Range Metamorphic Core Complex in eastern Nevada [*McCarthy*, 1986]. The origins of the reflectivity in these fault zones are likely to be similar to those of the Brevard. The shear wave reflectivity of these fault zones are also probably dependent on composition, structure, and frequency.

One must note that the simplest situation was described in this reflectivity study. Modeling the A cores assumes a uniform hydrostatic pressure, random orientation of fractures, and horizontally layered media. The field conditions for shear reflection profiling will contain some deviatoric stress fields and/or foliation which will produce a degree of shear wave splitting. The simple models suggest a need to use a more sophisticated type of modeling which would include nonnormal incidence and anisotropy. This study also suggests that continued studies of faults or shear zones are necessary to truly characterize the shear wave properties and reflectivity of mylonites. These future studies on shear wave properties should examine the detailed effects of anisotropy, compositional variations, and geologic structure on shear wave reflectivity. Finally, comparisons of compressional and shear wave properties will further our understanding of seismic imaging in mylonite zones.

Acknowledgments. We appreciate the comments and suggestions of D. Szymanski. We are grateful to D. Ballotti, C. Wilcox, and R. Baud for their assistance in data collection. We also thank M. Salisbury, L. Brown, and T. Brocher for their constructive reviews. This work was supported by the Office of Naval Research under contract N-00014-89-J-1209 (N.I. Christensen) and by a Purdue David Ross fellowship (C.L. McCaffree).

References

Aki, K., and P.G. Richards, *Quantitative Seismology: Theory and Methods*, v. I, pp. 123-192, W.H. Freeman, New York, 1980.

Alekseev, A.S, A.V. Egorkin, and N.I. Pavlenkova, Shear waves in the lithosphere studies on the territory of the U.S.S.R., *Tectonophysics, 154*, 227-239, 1988.

Birch, F., The velocity of compressional waves in rocks to 10 kilobars, 1, *J. Geophys. Res., 65*, 1083-1102, 1960.

Birch, F., The velocity of compressional waves in rocks to 10 kilobars, 2, *J. Geophys. Res., 66*, 2199-2224, 1961.

Christensen, N.I., Compressional wave velocities in metamorphic rocks at pressure to 10 kilobars, *J. Geophys. Res., 70*, 6148-6164, 1965.

Christensen, N. I., Shear wave velocities in metamorphic rocks at pressures to 10 kbar, *J. Geophys. Res., 71*, 3549-3556, 1966.

Christensen, N.I.; Seismic velocities, in *Handbook of Physical Properties*, v. II, edited by R.S. Carmichael, pp. 209-223, CRC Press, Boca Raton, Fla., 1982.

Christensen, N.I., The magnitude, symmetry and origin of upper mantle anisotropy based on fabric analyses of ultramafic tectonics, *Geophys. J. R. Astron. Soc., 76*, 89-111, 1984.

Christensen, N.I., Measurements of dynamic properties of rock at elevated temperatures and pressures, in *Measurements of Rock Properties at Elevated Pressures and Temperatures, ASTM STP 869*, edited by H.J. Pincus and E.R. Hoskins, pp. 93-107, American Society for Testing and Materials, Philadelphia, Pa., 1985.

Christensen, N.I., Reflectivity and seismic properties of the deep continental crust, *J. Geophys. Res., 94*, 17,793-17,804, 1989.

Christensen, N.I., and D.M. Fountain, Constitution of the lower continental crust based on experimental studies of seismic velocities in granulites, *Geol. Soc. Am. Bull., 86*, 227-236, 1975.

Christensen, N.I., and D.L. Szymanski, Origin of reflections from the Brevard Fault zone, *J. Geophys. Res., 93*, 1087-1102, 1988.

Christensen, N.I., and R.H. Wilkens, Seismic properties, density, and composition of the Icelandic crust near Reydarfjordur, *J. Geophys. Res., 87*, 6,389-6,395, 1982.

Claerbout, J.F., Synthesis of a layered medium from its acoustic transmission response, *Geophysics, 33*, 264-269, 1968.

Clark, H.B., J.K. Costain, and L. Glover, III, Structural and seismic reflection studies of the Brevard ductile deformation zone near Rossman, North Carolina, *Am. J. Sci., 278*, 419-441, 1978.

Cook, F.A., L.D. Brown, S. Kaufman, J.E. Oliver, and T.A. Peterson, COCORP seismic profiling of the Appalachian orogen beneath the Coastal Plains of Georgia, *Geol. Soc. Am. Bull., 92*, 738-748, 1981.

Cook, F.A., L.D. Brown, S. Kaufman, and J.E. Oliver, The COCORP seismic reflection traverse across the southern Appalachians, *AAPG Stud. Geol., 14*, 61, 1983.

Coruh, C., J.K. Costain, R.D. Hatcher, Jr., T.L. Pratt, R.T. Williams, and R.A. Phinney, Results from regional Vibroseis profiling: Appalachian ultradeep core hole site study, *Geophys. J.R. Astron. Soc., 89*, 147-155, 1987.

Crampin, S., Evaluation of anisotropy by shear-wave splitting, *Geophysics, 50*, 142-152, 1985.

Edelmann, H.K.A., and K. Helbig, Shear-waves surveys: Some aspects of field layout, in *Shear-Wave Exploration*, Geophys. Dev. Ser., v. 1, edited by S. H. Danbom and S.N. Domenico, pp 39-47, Society of Exploration Geophysicists, Tulsa, Okla., 1989.

Edelman, S.H., A. Liu, and R.D. Hatcher, Jr., The Brevard Zone in South Carolina and adjacent areas: An Alleghanian orogen-scale dextral shear zone reactivated as a thrust fault, *J. Geol., 95*, 793-806, 1987.

Griffin, V.S., Analysis of the Piedmont in northwest South Carolina, *Geol. Soc. Am. Bull., 85*, 1123-1138, 1974.

Goodwin, E.B., G.A. Thompson, and D.A. Okaya, Seismic identification of basement reflectors: the Bagdad reflection sequence in the Basin and Range Province-Colorado Plateau transition zone, Arizona, *Tectonics, 8*, 821-831, 1989.

Hatcher, R.D., Jr., Stratigraphy, petrology and structure of the Low Rank Belt and part of the Blue Ridge of northwesternmost South Carolina, *Geol. Notes S.C. Geol. Surv., 13*, 105-141, 1968.

Hatcher, R.D., Jr., Stratigraphy of the Brevard zone and Poor Mountain area Northwestern South Carolina, *Geol. Soc. Am. Bull., 81*, 933-940, 1970.

Hatcher, R.D., Jr., Stratigraphic, petrologic, and structural evidence favoring a thrust solution to the Brevard problem, *Am. J. Sci., 270*, 177-202, 1971.

Hatcher, R.D., Jr., J.K. Costain, C. Coruh, R.A. Phinney, and R.T. Williams, Tectonic implications of new Appalachian Ultradeep Core Hole (ADCOH) seismic reflection data from the crystalline southern Appalachians, *Geophys. J. R. Astron. Soc., 89*, 157-169, 1987.

Horton, J.W., Jr., Geologic map of the Rosman Quadrangle, North Carolina, *N. C. Dept. Nat. Res. Commun., Dev. Map MRS 185-NE*, Raleigh, 1982.

Hubbard, S.S., C. Coruh, and J.K. Costain, Paleozoic and Grenvillian structures in the southern Appalacians: Extended interpretation of seismic reflection data, *Tectonics, 10*, 141-170, 1991.

Hurich, C.A., and S.B. Smithson, Compositional variation and origin of deep crustal reflections, *Earth Planet. Sci. Lett., 85*, 416-426, 1987.

Jonas, A.I., Structure of metamorphic belt of the Southern Appalachians, *Am. J. Sci., 224*, 228-243, 1932.

Keith, A., Description of the Mount Mitchell quadrangle (North Carolina-Tennessee), in *Geological Atlas*, Folio 124, p. 10, U.S. Geological Survey, Reston, Va., 1905.

Layotte, P.C., MARTHOR: An S-wave impulse source, in *Shear-Wave Exploration*, Geophys. Dev. Ser., v. 1, edited by S. H. Danbom and S.N. Domenico, pp. 79-96, Society of Exploration Geophysicists, Tulsa, Okla., 1989.

Matthews, D. H., and M. J. Cheadle, Deep reflections from the Caledonides and comparison with the Himalayas, in *Reflection Seismology: A Global Perspective*, AGU, Geodyn. Ser., v. 13, edited by M.Barazang and L. Brown, pp. 5-20, Washington D.C., 1986.

McCarthy, J., Reflection profiles from the Snake Range Metamorphic Core Complex: A window into the mid-crust, in *Reflection Seismology: The Continental Crust*, AGU, Geodyn. Ser., v. 14, edited by M.Barazang and L. Brown, pp. 281-292, Washington D.C., 1986.

McCormack, M.D., J.A. Dunbar, and W.W. Sharp, A case study of stratigraphic interpretation using shear and compressional seismic data, *Geophysics, 49*, 505-520, 1984.

Reed, J.C., Jr., and B.H. Bryant, Evidence for strike-slip faulting along the Brevard zone in North Carolina, *Geol. Soc. Am. Bull., 75*, 1177-1196, 1964.

Robinson, E.A., and S. Treitel, The fine structure of the normal incidence synthetic seismogram, *Geophys. J. Astron. Soc., 53*, 289-309, 1977.

Roper, P.J., and P.S. Justus, Polytectonic evolution of the Brevard zone, *Am. J. Sci., 273A*, 105-132, 1973.

Ruter, H., and R. Schepers, Investigation of the seismic response of cyclically layered carboniferous rock by means of synthetic seismograms, *Geophys. Prospect., 26*, 29-41, 1978.

Schoenberger, M., and F.K. Levin, The effect of subsurface sampling on one-dimensional synthetic seismogram, *Geophysics, 44* , 1813-1829, 1979.

Siegesmund, S., H. Kern, and A. Vollbrecht, The effect of oriented microcracks on seismic velocities in an ultramylonite, *Tectonophysics, 186*, 241-251, 1991.

Smithson, S.B., J.A. Brewer, S. Kaufman, J.E. Oliver, and C.A. Hurich, Structure of the Laramide Wind River Uplift, Wyoming, from COCORP deep reflection data and from gravity data, *J. Geophys. Res., 84*, 5955-5973, 1979.

Wang, C., D.A. Okaya, C. Ruppert, G.A. Davis, T. Guo, Z. Zhong, and H.R. Wenk, Seismic reflectivity of the Whipple Mountain shear zone in southern California, *J. Geophys. Res., 94*, 2989-3005, 1989.

Ward, G., and M. Warner, Shear wave seismic reflections from the lower continental crust, *Eos Trans. AGU, 70*(43), 1203, 1989.

White, W.A., Blue Ridge front-A fault scarp, *Geol. Soc. Am. Bull., 71*, 1309-1346, 1950.

Widess, M.B., How thin is a thin bed?, *Geophysics, 46*, 1176-1180, 1973.

Wilkens, R., G. Simmons, and L. Caruso, The Vp/Vs as a discriminant of composition for siliceous limestones, *Geophysics, 49*, 185-196, 1984.

Williams, R.T., D.R. Hatcher, Jr., C. Coruh, J.K. Costain, M.D. Zoback, R.N. Anderson, J.B. Diebold, and R.A. Phinney, The southern Appalachian ultradeep scientific drill hole: Progress of site location investigations and other recent developments, in *Observations of the Continental Crust through Drilling*, v. 2, edited by H.J. Behr, F.G. Stanely, and H. Vidal, pp. 44-55, Springer-verlag, New York, 1987.

Wuenschel, P.C., Seismogram synthesis including multiples and transmission coefficients, *Geophysics, 25*, 106-129, 1960.

N. I. Christensen and C. L. McCaffree, Purdue University, Department of Earth and Atmospheric Sciences, 1397 Civil Engineering Building, West Lafayette, IN 47907-1397.

(Received February 28, 1992;
revised September 3, 1992;
accepted September 16, 1992.)